

DELFT UNIVERSITY OF TECHNOLOGY

MASTER'S THESIS

Topology of a Cooper Pair Transistor

by

Radoica Draškić

*A thesis submitted in fulfillment of the requirements
for the degree of Master of Science in Applied Physics
to be defended publicly on*

May 27, 2021

Student number: 5042674
Project duration: October 5, 2020 - April 4, 2021
Thesis committee: Prof. Anton AKHMEROV TU Delft, supervisor
Prof. Michael WIMMER TU Delft
Prof. Gary STEELE TU Delft
Daily supervisors: Dr. Valla FATEMI Yale University
M.Sc. Kostas VILKELIS TU Delft



Abstract

Superconducting quantum circuits came out as promising candidates for the exploration of topological phenomena that are currently inaccessible in condensed matter systems. One such circuit is a Cooper pair transistor which has already been widely studied in different regimes of operation due to its importance in quantum computation. However, it has only recently been appreciated that a Cooper pair transistor hosts a non-trivial Chern number and topologically protected current switching behavior. We provide here a more detailed analysis of Cooper pair transistor operation for different parameter regimes and explore the quantized ac current.

Acknowledgements

I would like to thank my supervisors Anton Akhmerov, Valla Fatemi, and Kostas Vilkelis for their invaluable guidance and support during the course of this project, and André Melo for useful discussions and for helping me find bugs in my code. Thanks to my family and my fiancé Nevena for their love and support. Finally, I am grateful for the funding received through TU Delft Excellence scholarship and Holland scholarship.

Contents

Abstract	iii
Acknowledgements	v
1 Introduction	1
1.1 Circuit Quantum Electrodynamics	1
1.2 Calculating Circuit Response	2
2 Quantized Current Response	5
2.1 Chern Number	5
2.2 Adiabatic Current	6
2.3 DC-biased Josephson Junctions	7
2.4 AC-biased Josephson Junctions	8
2.4.1 Extreme Asymmetry Limit, $\kappa \ll 1$	8
2.4.2 Transmon Regime, $E_J \gg E_C$	9
2.4.3 Intermediate Regime, $E_C \sim E_J$	11
2.4.4 Deep Charging Regime, $E_C \gg E_J$	13
3 Conclusion	15
A Current Divider	17
B Berry Curvature Properties	19
B.1 Berry Curvature in the Transmon Regime	20
C Response Quantization	23
Bibliography	25

1 Introduction

Topological phases and their classification are integral parts of the modern understanding of condensed matter systems. The usual object in the research of topological phases is the electronic matter that can exhibit a vast range of topological phenomena. However, the experimental realization of these materials is an arduous effort and detection of topological effects is difficult. Fortunately, materials are not the only platform for the exploration of topological phenomena and many artificial systems can exhibit non-trivial topological behavior. Superconducting quantum circuits with Josephson junctions are a well-developed technology and provide great flexibility and tunability [17] which makes them promising candidates for the exploration of topological phenomena. The topology of such circuits has already been studied from different aspects [6, 7, 12, 14], and thanks to their topological properties they have been proposed for novel technological applications such as standards in metrology [14, 15].

One of the simplest superconducting circuits is a Cooper pair transistor (CPT) which has been studied to a great extent due to its relevance to quantum computing [2, 3, 18], but it has only recently been appreciated that it exhibits a non-trivial Chern number and topologically protected current switching behavior [9]. There are, however, several questions regarding the exactness of the current quantization, the response to ac signals and the choice of circuit parameters that have still not been considered. We will analyze the topological properties of a CPT in more detail and answer these questions in different regimes of operation of the device.

1.1 Circuit Quantum Electrodynamics

Circuit quantum electrodynamics (cQED) is a formalism used in the description of the interaction between light and matter in superconducting quantum circuits [4, 5]. The usual steps in the description include writing down the circuit Lagrangian followed by the construction of the corresponding circuit Hamiltonian that can further be cast into its second quantized form depending on the regime of interest. Here we will go straight to the definition of the CPT Hamiltonian, but an interested reader can follow through the procedure presented in [4].

The circuit of a Copper pair transistor consists of two Josephson junctions connected in series with energies E_{JL} and E_{JR} forming a charge island, which is capacitively biased by a gate voltage V_g through a capacitor of capacitance C , as shown in the Fig. 1.1. The circuit Hamiltonian is then given by

$$\hat{\mathcal{H}}(n_g, \varphi_L, \varphi_R) = E_C(\hat{n} - n_g)^2 - E_{JL} \cos(\hat{\varphi} - \varphi_L) - E_{JR} \cos(\hat{\varphi} - \varphi_R), \quad (1.1)$$

where \hat{n} is a Cooper pair number operator of the island and $\hat{\varphi}$ is its canonically conjugated phase operator such that canonical commutation relation $[\hat{\varphi}, \hat{n}] = i$ holds. Phases applied through voltages at the ends of the left and right Josephson junction are given by φ_L and φ_R respectively. The charging energy $E_C = (2e)^2/2C$ represents the energy scale of adding Cooper pairs to the island, and the offset charge is given by $n_g = -CV_g/2e$.

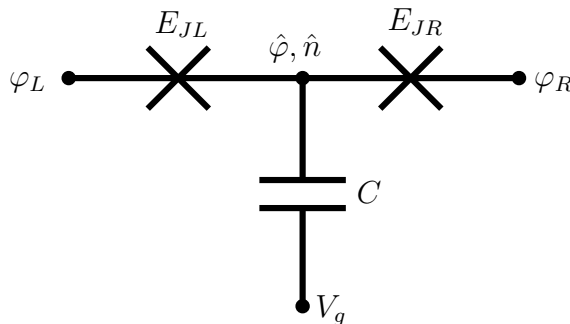


FIGURE 1.1: Circuit of the Cooper pair transistor. Two Josephson junctions are described by the energies E_{JL} and E_{JR} . The island is described by its Cooper pair number and phase operators \hat{n} , $\hat{\varphi}$. Circuit is driven by applying the voltage V_g on the capacitor C and a voltage across the Josephson junctions such that $\varphi_{L/R} = 2eV_{L/R}/\hbar$.

In general, there are always capacitances associated with every Josephson junction that can be modeled as being connected in parallel with the corresponding Josephson junction, but we omit them here in order to simplify our analysis since they don't affect our conclusions. We also note that there is a dual way to represent the Cooper pair transistor using the Quantum phase slip element [13] and an inductor where the roles of Cooper pair number and phase operators are exchanged, i.e. there is a tunneling of flux quanta across the element instead of Cooper pairs

$$\hat{\mathcal{H}}(\varphi_g, n_L, n_R) = E_L(\hat{\varphi} - \varphi_g)^2 - E_{QL} \cos(2\pi(\hat{n} - n_L)) - E_{QR} \cos(2\pi(\hat{n} - n_R)). \quad (1.2)$$

Due to different advances in Josephson junction and Quantum phase slip technologies, it might be worth considering this alternative implementation depending on the desired ratio of characteristic energies E_J/E_C or E_Q/E_L .

1.2 Calculating Circuit Response

Measurements of topological properties of superconducting circuits can be done through transconductance measurements [7, 16]. We are interested in the current response of our circuit under the change of parameters n_g , φ_L , and φ_R , and Berry curvature is a required formalism for its description so we will explain it in the following paragraphs.

In quantum mechanical systems the Berry curvature arises when a system undergoes an adiabatic evolution [8]. Let's consider a Hamiltonian $\hat{\mathcal{H}}(\mathbf{R}(t))$

that depends on some vector of parameters \mathbf{R} , which in turn depend on time t , together with the set of its instantaneous eigenstates $|\psi_n(\mathbf{R}(t))\rangle$ and eigenvalues $E_n(\mathbf{R}(t))$. If the eigenvalue $E_n(\mathbf{R}(t))$ remains non-degenerate everywhere along the path in the parameter space and the variation with time of the parameters is slow enough, then the adiabatic theorem states that a system initially in the eigenstate $|\psi_n(\mathbf{R}(0))\rangle$ will stay in the instantaneous eigenstate $|\psi_n(\mathbf{R}(t))\rangle$ at time t , up to a global phase, i.e. the state is given by

$$|\Psi_n(t)\rangle = e^{i\gamma_n(t)} e^{-\frac{i}{\hbar} \int_0^t dt' E_n(\mathbf{R}(t'))} |\psi_n(\mathbf{R}(t))\rangle. \quad (1.3)$$

The second exponential term is the dynamical phase while the first exponential term is the geometric phase where γ_n is the Berry phase

$$\gamma_n(t) = i \int_0^t dt' \langle \psi_n(\mathbf{R}(t')) | \frac{d}{dt'} |\psi_n(\mathbf{R}(t'))\rangle = i \int_{\mathbf{R}(0)}^{\mathbf{R}(t)} d\mathbf{R} \langle \psi_n(\mathbf{R}) | \nabla_{\mathbf{R}} |\psi_n(\mathbf{R})\rangle. \quad (1.4)$$

It is usually more insightful to consider the integrand in the previous expression which is known as the Berry connection $\mathcal{A}_n(\mathbf{R}) = i \langle \psi_n(\mathbf{R}) | \nabla_{\mathbf{R}} |\psi_n(\mathbf{R})\rangle$. Then, one can define Berry curvature, which is an anti-symmetric second rank tensor derived from Berry connection, as

$$B_n^{\mu\nu}(\mathbf{R}) = \frac{\partial}{\partial R_\mu} \mathcal{A}_n^\nu(\mathbf{R}) - \frac{\partial}{\partial R_\nu} \mathcal{A}_n^\mu(\mathbf{R}) = -2\text{Im} \langle \partial_{R_\mu} \psi_n | \partial_{R_\nu} \psi_n \rangle. \quad (1.5)$$

Berry curvature can also be written as a summation over the eigenstates [19]

$$B_n^{\mu\nu} = i \sum_{m \neq n} \frac{\langle \psi_m | \partial \hat{\mathcal{H}} / \partial R_\mu | \psi_n \rangle \langle \psi_n | \partial \hat{\mathcal{H}} / \partial R_\nu | \psi_m \rangle - (\nu \leftrightarrow \mu)}{(E_m - E_n)^2}, \quad (1.6)$$

which is usually more useful for numerical calculations.

Finally, to measure the circuit response we have to define the current operators for both branches of the Cooper pair transistor

$$\hat{I}_{L/R} = \frac{2e}{\hbar} \frac{\partial \hat{\mathcal{H}}}{\partial \varphi_{L/R}}. \quad (1.7)$$

Then the expectation value in the k -th band is given to the first order by

$$I_{L/R,k} = \frac{2e}{\hbar} \frac{\partial E_k}{\partial \varphi_{L/R}} - 2e\dot{n}_g B_k^{\varphi_{L/R} n_g} - 2e\dot{\varphi}_{R/L} B_k^{\varphi_{L/R} \varphi_{R/L}}. \quad (1.8)$$

If we ground the opposite Josephson junction then the third term in the previous equation does not contribute. In our numerical experiments, we are using the formula from Eq. 1.6 in order to numerically calculate Berry curvature, however, we also note that in the case of CPT one can also do this using the properties of Mathieu functions as described in the Appendix B.

2 Quantized Current Response

Quantization of current response is a distinctive feature of the CPT and has been previously discussed in [9] where a specific measurement protocol is proposed for measuring quantized dc current. Ideal quantized dc current response, where current flows through only one of the Josephson junctions, requires a linear increase of the offset charge n_g through the linear increase of the gate voltage V_g . However, this is practically impossible since the capacitor would eventually break. To go around this problem, the protocol proposed in [9] requires a periodic linear increase and decrease of the voltage applied to the capacitor accompanied by the change of the ratio of Josephson energies using the external magnetic flux.

Since the previously mentioned protocol effectively applies an ac signal to the capacitor, we are inspired to consider a sinusoidal signal on the capacitor, albeit, without changing the ratio of Josephson energies. This results in the quantization of the corresponding ac component on the output terminal and in this chapter we will explore this quantization in different regimes and shed more light on the amount of deviation from the perfect quantization.

Throughout this chapter we will set $E_{JL} \equiv E_J$, $E_{JR} \equiv \kappa E_J$, and consider only the regimes when $0 \leq \kappa < 1$ for convenience, unless stated otherwise. We also assume that voltages and frequencies appearing throughout the chapter are sufficiently low such that the adiabatic theorem applies and that the system is always in the ground state. We will write $B^{\alpha\beta}$ instead of $B_0^{\alpha\beta}$ for brevity and will always assume that the right Josephson junction is grounded $\varphi_R = 0$ so that the term proportional to $B^{\varphi_L\varphi_R}$ does not contribute to the output current.

2.1 Chern Number

The spectrum of the CPT has a non-zero Berry curvature $B_k^{\varphi_L/Rn_g}$ which is a consequence of Weyl points in the 3D space spanned by the parameters $(n_g, \varphi_L - \varphi_R, E_{JL} - E_{JR})$. For fixed $E_{JL} - E_{JR}$, Berry curvature is periodic in n_g and $\varphi_L - \varphi_R$ so we can consider $(n_g, \varphi_L - \varphi_R) \in [0, 1] \times [0, 2\pi]$ as quasi-momenta spanning the Brillouin zone and we can define a corresponding Chern number. As demonstrated in [9], depending on which of the Josephson energies is larger, the Chern number

$$C_k^{n_g\varphi_L/R} = \frac{1}{2\pi} \int_0^{2\pi} d\varphi_{L/R} \int_0^1 dn_g B_k^{n_g\varphi_L/R}, \quad (2.1)$$

is either 0 or 1 for all bands k .

Chern number is a central concept in the description of the quantized current response and, in an ideal setting, currents through the device would be

related as $I_{L/R,k} = C_k^{n_g \varphi_{L/R}} I_g$. Here, $I_g = 2e\dot{n}_g$ is a displacement current entering through the capacitor and $I_{L/R,k}$ is a current that is leaving through the corresponding Josephson junction. Since $C_k^{n_g \varphi_{L/R}}$ is either 0 or 1 depending on the sign of $E_{JL} - E_{JR}$, current entering through the capacitor exits only through the junction with larger Josephson energy. In the following sections, we will only explore the current response through the larger Josephson junction, however, the entire analysis can easily be extended to the other Josephson junction. Also, the nonlinearity of Josephson junctions is critical for the existence of a non-trivial Chern number in a CPT and similar behavior is unobtainable if the Josephson junctions are replaced by inductors, even though the formalism of Berry curvature is required for a proper quantum mechanical description (see Appendix A).

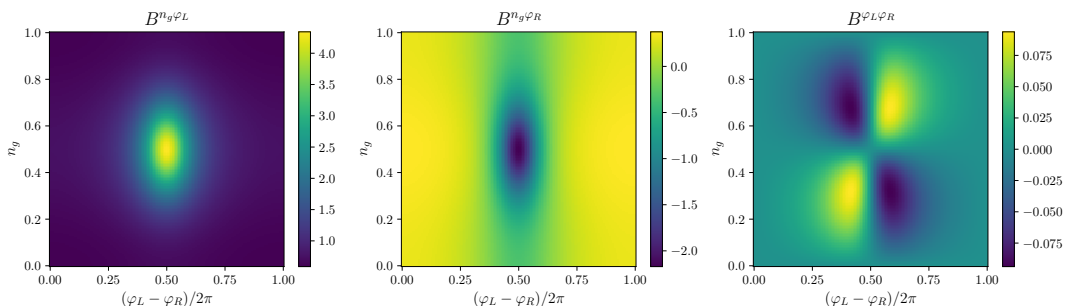


FIGURE 2.1: Berry curvature of the CPT for $E_J/E_C = 1$ and $\kappa = 0.5$. From left to right, the Chern numbers are $C^{n_g \varphi_L} = 1$, $C^{n_g \varphi_R} = 0$, and $C^{\varphi_L \varphi_R} = 0$.

2.2 Adiabatic Current

Adiabatic current represents the first term in the Eq. 1.8 and it does not contribute to the quantized response. This current is proportional to the energy derivative which is given by

$$\frac{\partial E_m}{\partial \varphi_{L/R}} = \frac{\kappa E_J \sin(\varphi_{L/R} - \varphi_{R/L})}{2\sqrt{1 + \kappa^2 + 2\kappa \cos(\varphi_L - \varphi_R)}} \times a'_{2[n_g + k(m, n_g)]} \left(-\frac{2E_J}{E_C} \sqrt{1 + \kappa^2 + 2\kappa \cos(\varphi_L - \varphi_R)} \right), \quad (2.2)$$

where $a_\nu(q)$ denotes Mathieu's characteristic value, $a'_\nu(q)$ its derivative with respect to q , and $k(m, n_g)$ is a function appropriately sorting the eigenvalues (see Appendix B). From the previous formula it follows that $\partial_{\varphi_{L/R}} E_m(n_g, \varphi_L - \varphi_R) = -\partial_{\varphi_{L/R}} E_m(n_g, \pi - \varphi_L + \varphi_R)$. Due to this symmetry, the energy derivative integrates to zero over the Brillouin zone.

In all of the regimes that we are considering, the leading order of the adiabatic current response is proportional to this integral hence it vanishes. Because

of this, we will not analyze this contribution in detail. However, it might become relevant in the regimes when the condition $I_g \gg 2eE_J/\hbar$ is not satisfied or for different sweeps of the Brillouin zone which we leave for future work.

2.3 DC-biased Josephson Junctions

We will first consider a somewhat simpler case where we apply a dc voltage V_0 across the Josephson junctions, such that the phase difference is given by $\varphi_L - \varphi_R = 2eV_0t/\hbar \equiv \omega_0t$, and an ac signal on the capacitor of the form $n_g = r_g \cos(\omega_g t)$. If the ratio ω_g/ω_0 is irrational, the current quantization is given by (see Appendix C)

$$\frac{I_L(\omega_g)}{I_g(\omega_g)} = 1 + \sum_{n=1}^{+\infty} \frac{1}{n\pi r_g} a_n J_1(2n\pi r_g), \quad (2.3)$$

where J_1 is a Bessel function and a_n are Fourier cosine series coefficients of the Berry curvature given by

$$a_n(\kappa, E_J/E_C) = \frac{1}{\pi} \int_0^{2\pi} d\phi \int_0^1 dx \cos(2\pi n x) B^{n_g \varphi_L}(n_g = x, \varphi_L - \varphi_R = \phi). \quad (2.4)$$

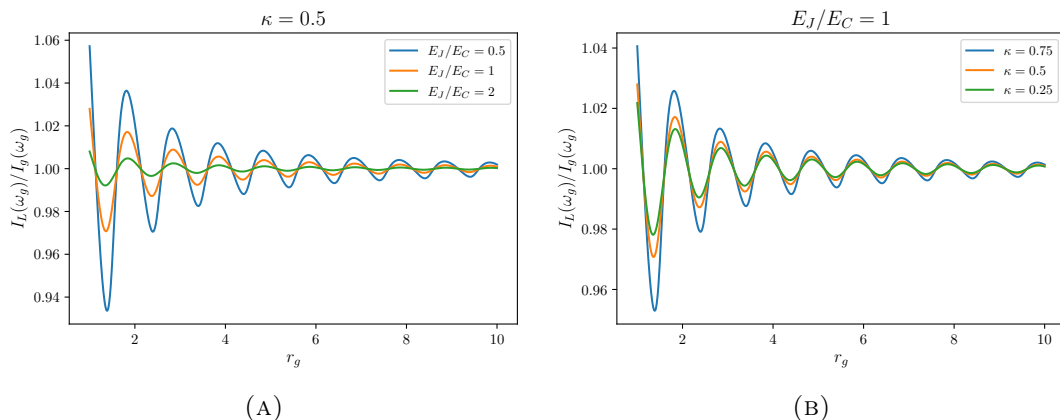


FIGURE 2.2: Current quantization in the case of dc-biased Josephson junctions when ω_g/ω_0 is irrational. (A) Quantization for different values of E_J/E_C ratio over the range of the sweep amplitudes r_g and $\kappa = 0.5$ displaying exponentially suppressed oscillations. (B) Quantization for different values of κ over the range of the sweep amplitudes r_g and $E_J/E_C = 1$.

The response quantization can be well approximated by (Fig. 2.2)

$$\frac{I_L(\omega_g)}{I_g(\omega_g)} \approx 1 + f(\kappa, E_J/E_C) \frac{1}{r_g^{3/2}} \sin(2\pi r_g + \alpha), \quad (2.5)$$

where α is a phase that depends on the circuit parameters. For large enough E_J/E_C , function $f(\kappa, E_J/E_C)$ contributes to the exponential decay of the correction as $e^{-\beta\sqrt{E_J/E_C}}$ such that in the transmon regime, when $E_J \gg E_C$, the

quantization becomes practically perfect. We also note that the quantization is perfect for particular values of r_g due to the term $\sin(2\pi r_g + \alpha)$.

In the case of a rational $\omega_g/\omega_0 = p/q$ the quantization is not always perfect in the limit $r_g \rightarrow \infty$ (Fig. 2.3). However, one can arbitrarily approach perfect quantization for sufficiently large p and q .

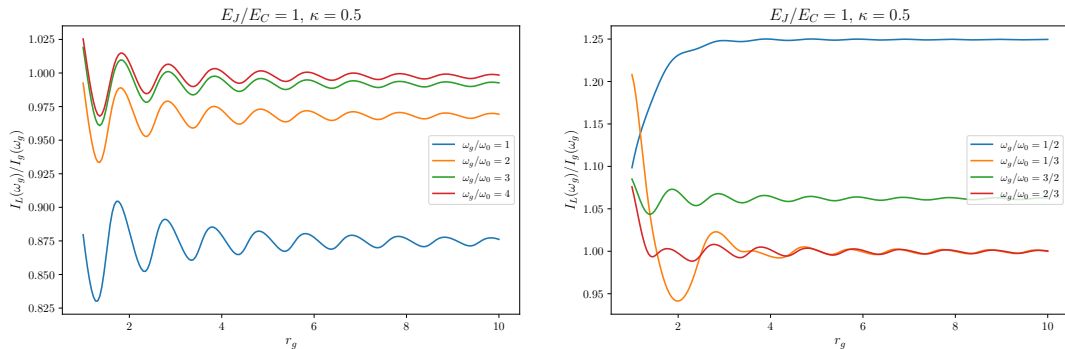


FIGURE 2.3: Current quantization in the case of dc-biased Josephson junctions when ω_g/ω_0 is rational over the range of the sweep amplitudes r_g and $E_J/E_C = 1$, $\kappa = 0.5$. The quantization does not approach the perfect value as $r_g \rightarrow \infty$ but can be improved arbitrarily by the appropriate choice of p and q .

2.4 AC-biased Josephson Junctions

Another regime that we consider is when an ac voltage is applied across the Josephson junctions $\varphi_L - \varphi_R = 2\pi r_\varphi \cos(\omega_0 t)$ together with an ac signal on the capacitor $n_g = r_g \cos(\omega_g t)$. Again, if the ratio ω_g/ω_0 is irrational, the quantization is given by (see Appendix C)

$$\frac{I_L(\omega_g)}{I_g(\omega_g)} = 1 + \sum_{m=1}^{+\infty} a_{0m} J_0(2m\pi r_\varphi) + \sum_{n=1, m=0}^{+\infty} \frac{1}{n\pi r_g} a_{nm} J_1(2n\pi r_g) J_0(2m\pi r_\varphi), \quad (2.6)$$

where a_{nm} are Fourier cosine series coefficients of the Berry curvature. However, the most general analysis of this expression is not straightforward so we will focus on some specific parameter regimes in order to characterize the device's behavior. We also consider the case $\omega_g/\omega_0 = 1$ where the quantization is also expected to be perfect under certain conditions.

2.4.1 Extreme Asymmetry Limit, $\kappa \ll 1$

In this regime the Berry curvature effectively stops depending on the phase difference across Josephson junctions $\varphi_L - \varphi_R$ and only depends on the offset charge n_g . In the limit $\kappa \rightarrow 0$, Cooper pair transistor reduces to a Cooper pair box (CPB), i.e. a circuit with only one Josephson junction and a capacitor. CPB can be considered as the smallest circuit with topological effects due to nonvanishing Berry curvature.

Since there is no dependence on $\varphi_L - \varphi_R$, the Fourier series coefficients of the Berry curvature from the Eq. 2.6 are of the form $a_{nm} = a_n \delta_{m0}$, so the current quantization is given by

$$\frac{I_L(\omega_g)}{I_g(\omega_g)} = 1 + \sum_{n=1}^{+\infty} \frac{1}{n\pi r_g} a_n J_1(2\pi n r_g), \quad (2.7)$$

for any ω_g/ω_0 . This formula for the current quantization is the same as the one in the case of dc-biased Josephson junctions when $\kappa = 0$. Similarly to the asymptotic analysis given by Eq. 2.5, we have that the asymptotic behavior is well described by (Fig. 2.4)

$$\frac{I_L(\omega_g)}{I_g(\omega_g)} \approx 1 + f(E_J/E_C) \frac{1}{r_g^{3/2}} \sin(2\pi r_g + \alpha). \quad (2.8)$$

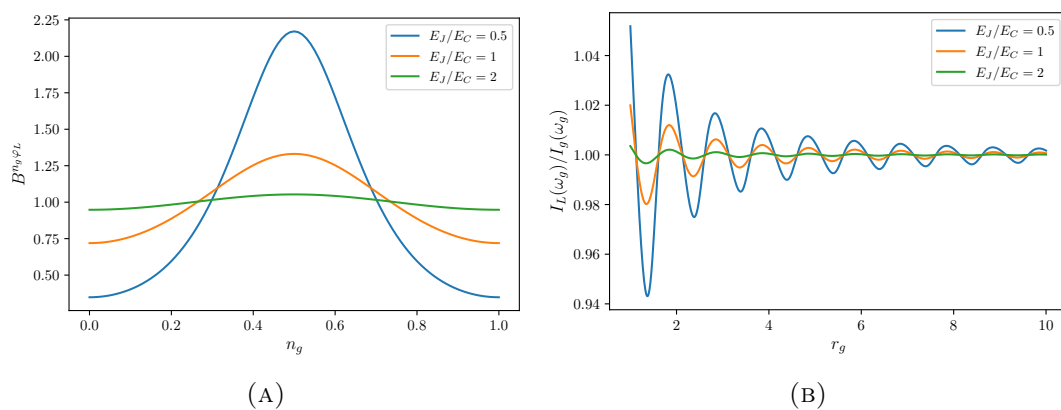


FIGURE 2.4: Current quantization in the extreme asymmetry limit for the ac-biased Josephson junctions. (A) Berry curvature of the CPB which is a good approximation of the CPT when $\kappa \ll 1$. In this regime only the dependence on the offset charge n_g remains. (B) Current quantization for different values of E_J/E_C ratio over the range of the sweep amplitudes r_g and $\kappa = 0$. The amplitude of the oscillations decreases with the power law $r_g^{-3/2}$ and exponentially in $\sqrt{E_J/E_C}$.

2.4.2 Transmon Regime, $E_J \gg E_C$

In the transmon regime, when $E_J \gg E_C$, Josephson junctions become nearly classical. In the ground state, the phase across the Josephson junction with larger characteristic energy is approximately zero since the corresponding term in the Hamiltonian makes a dominant contribution to the minimum of potential energy. This in turn qualitatively describes the tendency of the current to only flow through the larger Josephson junction.

The ground state is localized at the bottom of the potential well and closely resembles the ground state of a harmonic oscillator. Berry curvature can then be obtained by a simplified calculation and to the lowest order it is given by (see Appendix B.1)

$$B^{n_g \varphi_L} = \frac{1 + \kappa \cos(\varphi_L - \varphi_R)}{1 + \kappa^2 + 2\kappa \cos(\varphi_L - \varphi_R)}. \quad (2.9)$$

We see that the Berry curvature does not depend on the offset charge n_g which simplifies our analysis.

We can expand the Berry curvature into a series in terms of κ as (see Appendix B.1)

$$B^{n_g \varphi_L} = \sum_{m=0}^{\infty} (-1)^m \kappa^m \cos(m(\varphi_L - \varphi_R)), \quad (2.10)$$

and read out the Fourier coefficients $a_{nm} = (-1)^m \kappa^m \delta_{n0}$. Plugging this into the Eq. 2.6, we obtain the formula for the current quantization for any ω_g that is not an integer multiple of ω_0

$$\frac{I_L(\omega_g)}{I_g(\omega_g)} = 1 + \sum_{n=1}^{+\infty} (-1)^n \kappa^n J_0(2n\pi r_\varphi). \quad (2.11)$$

This time, current quantization is well approximated by (Fig. 2.5)

$$\frac{I_L(\omega_g)}{I_g(\omega_g)} \approx 1 + f(\kappa) \frac{1}{\sqrt{r_\varphi}} \sin(2\pi r_\varphi + \alpha), \quad (2.12)$$

for sufficiently low values of κ .

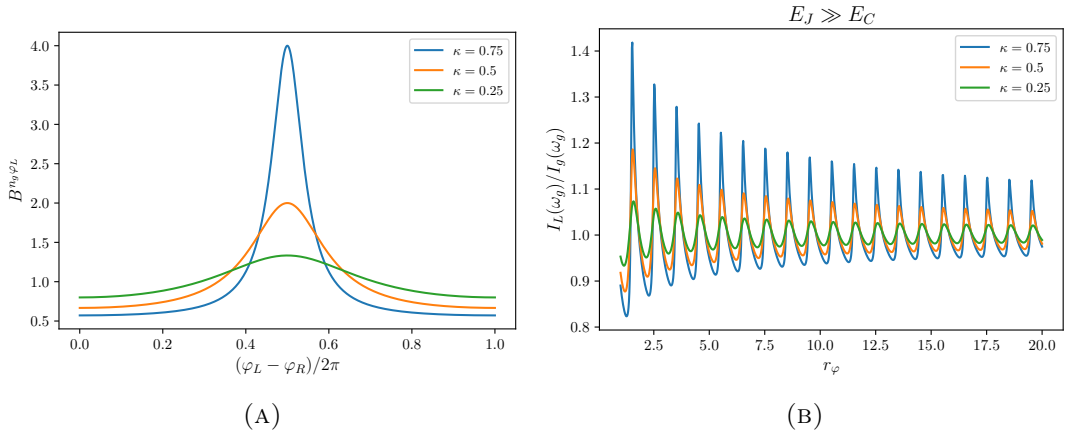


FIGURE 2.5: (A) Berry curvature in the transmon regime for different values of κ depending only on the phase difference across the Josephson junctions. (B) Current quantization for different values of κ . The amplitude of oscillations around the perfect quantization decreases as $r_\varphi^{-1/2}$.

In the case when $\omega_g = p\omega_0$ for an integer p , the current quantization has an additional contribution

$$\frac{I_L(\omega_g)}{I_g(\omega_g)} = 1 + \sum_{n=1}^{+\infty} (-1)^n \kappa^n (J_0(2n\pi r_\varphi) - (-1)^p J_{2p}(2n\pi r_\varphi)), \quad (2.13)$$

which influences the decay of the oscillations (Fig. 2.6), and in this case it is well approximated by

$$\frac{I_L(\omega_g)}{I_g(\omega_g)} \approx 1 + f(\kappa) \frac{1}{r_\varphi^{3/2}} \sin(2\pi r_\varphi + \alpha). \quad (2.14)$$

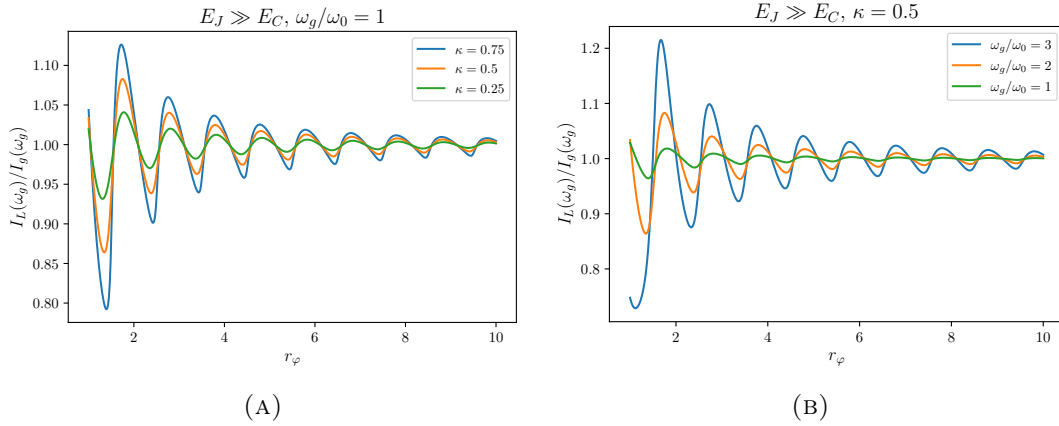


FIGURE 2.6: Current quantization in the transmon regime when $\omega_g = p\omega_0$. In this case the oscillations decay as $r_\varphi^{-3/2}$. (A) Quantization for $p = 1$ and different values of κ over the range of the sweep amplitudes r_φ . (B) Quantization for $\kappa = 0.5$ and different values of p .

2.4.3 Intermediate Regime, $E_C \sim E_J$

In the intermediate regime, when $E_C \sim E_J$, the dependence of the Berry curvature on the phase difference $\varphi_L - \varphi_R$ and the offset charge n_g is nontrivial, hence all of the terms in Eq. 2.6 are contributing in the expression for the current quantization.

Current quantization given by Eq. 2.6 cannot be simplified in this case but can be well approximated by (Fig. 2.7)

$$\frac{I_L(\omega_g)}{I_g(\omega_g)} \approx 1 + f(E_J/E_C, \kappa) \frac{1}{r_g^{3/2} r_\varphi^{1/2}} \sin(2\pi r_g + \alpha) \sin(2\pi r_\varphi + \beta), \quad (2.15)$$

when ω_g/ω_0 is irrational.

In the case when $\omega_g/\omega_0 = 1$ the dependence of quantization on the signal amplitudes becomes more complicated. For rational ratios of amplitudes r_g/r_φ the path in parameter space wraps back onto itself and the Brillouin zone does not get sampled sufficiently for the proper integration of the Berry curvature and the quantization is not perfect. This results in the peaks in Fig. 2.8b which persist in spite of the increase in the signal amplitudes. Nevertheless, in the case of the irrational ratio r_g/r_φ , the quantization approaches the ideal value as the amplitude increases because this time the path through the Brillouin zone never repeats and the sampling of points is sufficient for the integration of the Berry curvature.

Other ratios of frequencies $\omega_g/\omega_0 = p/q$ do not necessarily result in a quantized response since the paths through the Brillouin zone become more complicated and much larger amplitudes might be required. However, for large enough p and q the quantization increasingly resembles the case of irrational ratio of frequencies.

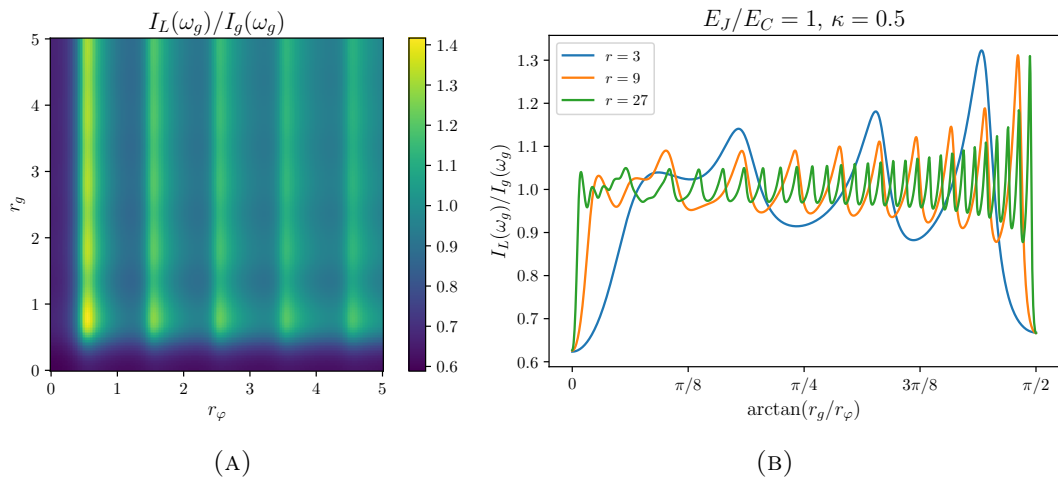


FIGURE 2.7: Current quantization in the intermediate regime for irrational ω_g/ω_0 and $E_J/E_C = 1$, $\kappa = 0.5$. (A) Quantization across r_g and r_φ . We observe that oscillations decay as $r_g^{-3/2}r_\varphi^{-1/2}$. (B) Quantization for different values of the sweep amplitude $r = \sqrt{r_g^2 + r_\varphi^2}$ and sweep angle $\arctan(r_g/r_\varphi)$ where we can also observe the decay of the deviation from perfect quantization.

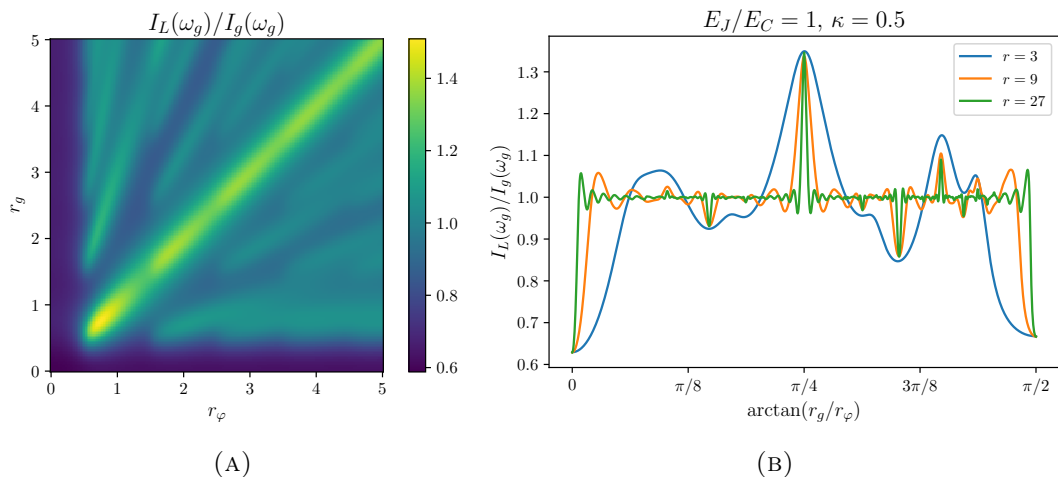


FIGURE 2.8: Current quantization in the intermediate regime for $\omega_g/\omega_0 = 1$, $E_J/E_C = 1$, and $\kappa = 0.5$. (A) Quantization across r_g and r_φ . (B) Current quantization for different values of sweep amplitude $r = \sqrt{r_g^2 + r_\varphi^2}$ and sweep angle $\arctan(r_g/r_\varphi)$. We see that peaks persist for rational values of r_g/r_φ since only the specific parts of the Brillouin zone are being sampled in that case. However, the overall trend indicates the decrease in the deviation from perfect quantization as $r \rightarrow \infty$.

2.4.4 Deep Charging Regime, $E_C \gg E_J$

In the deep charging regime, when $E_C \gg E_J$, we can reduce our analysis to the two lowest charge states $|0\rangle$ and $|1\rangle$ by considering the offset charge in the range $n_g \in [0, 1]$. The Hamiltonian is then given by

$$\hat{\mathcal{H}}(n_g, \varphi_L, \varphi_R) = -\frac{E_J}{2} \begin{pmatrix} \lambda(1 - 2n_g) & e^{i\varphi_L} + \kappa e^{i\varphi_R} \\ e^{-i\varphi_L} + \kappa e^{-i\varphi_R} & -\lambda(1 - 2n_g) \end{pmatrix}, \quad (2.16)$$

where we set $\lambda \equiv E_C/E_J$. This time, we can calculate the Berry curvature exactly

$$B^{n_g\varphi_L} = \frac{\lambda(1 + \kappa \cos(\varphi_L - \varphi_R))}{(\lambda^2(1 - 2n_g)^2 + 1 + \kappa^2 + 2\kappa \cos(\varphi_L - \varphi_R))^{3/2}} + o(\lambda^{-2}). \quad (2.17)$$

Using this formula for the Berry curvature, we can estimate the full width at half maximum (FWHM) along the n_g as $\text{FWHM}_{n_g} \sim (1 - \kappa)/\lambda$ and along the $\varphi_L - \varphi_R$ as $\text{FWHM}_\varphi \sim (1 - \kappa)^2/\sqrt{\kappa}$ for sufficiently large κ . Then the area of the Berry curvature hotspot scales as $A \sim \text{FWHM}_{n_g} \times \text{FWHM}_\varphi \sim (1 - \kappa)^3/\lambda\sqrt{\kappa}$. Knowing this, we can estimate the rate of convergence of the quantization with the radius of the sweep r in the case when $\omega_g/\omega_0 = 1$ since it depends on the faithful sampling of the Brillouin zone. In order to sample the Brillouin zone sufficiently, it is required that r_g/r_φ is irrational and that the spacing between sweep lines is much smaller than the linear dimension of the Berry curvature hotspot $1/r \ll \sqrt{A}$, or, written differently $r \gg 1/\sqrt{A}$. For example, if $\lambda = 10$ and $\kappa = 0.9$, then the area of the hotspot is of the order $A \sim 10^{-4}$, hence, the condition on the sweep amplitude is $r \gg 100$, i.e. we need to sweep hundreds of Brillouin zones to achieve low enough deviation from perfect quantization.

In the case when ω_g/ω_0 is irrational, error scaling from Section 2.4.3 still holds to a high accuracy, i.e. the amplitude of oscillations around the perfect quantization still decays as $r_g^{-3/2}r_\varphi^{-1/2}$ but increases with λ .

3 Conclusion

We explored the topological behavior of one of the simplest superconducting circuits, the Cooper pair transistor. We demonstrated a rich set of phenomena related to the exactness of the current quantization and the response of the circuit to the ac drive that have not been previously discussed. We hope that this analysis will help the experimental efforts in the search for suitable parameters like the signal amplitudes and characteristic energy scales to demonstrate the nontrivial topology of the CPT.

Possible future directions of research are further exploration of the current quantization with respect to the sweep angle and of more complicated forms of the input signal. Additional analysis of the constraints on frequencies and voltages with respect to adiabaticity is also required. It would also be interesting to explore whether one can define corresponding edge states by turning n_g and $\varphi_L - \varphi_R$ into dynamical variables [9].

A Current Divider

We present here the calculation of the current response in the case when Josephson junctions are replaced by inductors to showcase the importance of nonlinearity for the quantization of the response.

Let's start with the circuit Hamiltonian

$$\begin{aligned}\hat{\mathcal{H}}(n_g, \varphi_1, \varphi_2) &= E_C(\hat{n} - n_g)^2 + E_{L1}(\hat{\varphi} - \varphi_1)^2 + E_{L2}(\hat{\varphi} - \varphi_2)^2 \\ &\equiv E_C(\hat{n} - n_g)^2 + (E_{L1} + E_{L2})(\hat{\varphi} - \varphi_0)^2,\end{aligned}\quad (\text{A.1})$$

where $\varphi_0 = (E_{L1}\varphi_1 + E_{L2}\varphi_2)/(E_{L1} + E_{L2})$.

The ground state in the phase basis is given by

$$\psi_0(\varphi) = A e^{in_g(\varphi - \varphi_0)} e^{-\beta(\varphi - \varphi_0)^2}, \quad (\text{A.2})$$

where A and β are appropriate constants such that the wave function is properly normalized. In order to calculate the Berry curvature we have to calculate the necessary ground state derivatives

$$\frac{\partial \psi_0}{\partial n_g} = i(\varphi - \varphi_0)\psi_0, \quad (\text{A.3})$$

$$\frac{\partial \psi_0}{\partial \varphi_i} = \frac{\partial \varphi_0}{\partial \varphi_i} \frac{\partial \psi_0}{\partial \varphi_0} = \frac{E_{Li}}{E_{L1} + E_{L2}} (-in_g + 2\beta(\varphi - \varphi_0)) \psi_0. \quad (\text{A.4})$$

Berry curvature is then given by

$$\begin{aligned}B^{n_g \varphi_i} &= -2\text{Im} \langle \partial_{n_g} \psi_0 | \partial_{\varphi_i} \psi_0 \rangle \\ &= \frac{E_{Li}}{E_{L1} + E_{L2}} \times 4\beta \int_{-\infty}^{+\infty} d\varphi (\varphi - \varphi_0)^2 |\psi_0|^2 \\ &= \frac{E_{Li}}{E_{L1} + E_{L2}} \times 4\beta \int_{-\infty}^{+\infty} dx A^2 x^2 e^{-2\beta x^2} = \frac{E_{Li}}{E_{L1} + E_{L2}},\end{aligned}\quad (\text{A.5})$$

$$B^{\varphi_1 \varphi_2} = 0, \quad (\text{A.6})$$

where $i = 1, 2$.

Finally, the current response is given by

$$I_i = \frac{2e}{\hbar} \frac{\partial E_0}{\partial \varphi_i} - 2e\dot{n}_g B^{\varphi_i n_g} = 2e\dot{n}_g B^{n_g \varphi_i} = I_g \frac{E_{Li}}{E_{L2} + E_{L2}} = I_g \frac{L_{3-i}}{L_1 + L_2}, \quad (\text{A.7})$$

where $i = 1, 2$, which is a well known formula for the current divider.

B Berry Curvature Properties

We can rewrite the CPT Hamiltonian in the following way

$$\begin{aligned}\hat{\mathcal{H}}(n_g, \varphi_L, \varphi_R) &= E_C(\hat{n} - n_g)^2 - E_J \cos(\hat{\varphi} - \varphi_L) - \kappa E_J \cos(\hat{\varphi} - \varphi_R) \quad (\text{B.1}) \\ &= E_C(\hat{n} - n_g)^2 - E_J \sqrt{1 + \kappa^2 + 2\kappa \cos(\varphi_L - \varphi_R)} \cos(\hat{\varphi} - \varphi_0) \\ &\equiv E_C(\hat{n} - n_g)^2 - E_J(\kappa, \varphi_L, \varphi_R) \cos(\hat{\varphi} - \varphi_0(\kappa, \varphi_L, \varphi_R)),\end{aligned}$$

where

$$\varphi_0 = \arctan \frac{\sin \varphi_L + \kappa \sin \varphi_R}{\cos \varphi_L + \kappa \cos \varphi_R}. \quad (\text{B.2})$$

We see that the Hamiltonian is effectively reduced to the one of a circuit with a capacitor and a single Josephson junction, i.e. a Cooper pair box (CPB)

$$\hat{\mathcal{H}}(n_g, \varphi_0, E_J) = E_C(\hat{n} - n_g)^2 - E_J \cos(\hat{\varphi} - \varphi_0). \quad (\text{B.3})$$

We also note that this procedure can be performed for an arbitrary number of Josephson junctions connected to a single charge island.

It turns out that for a CPB Hamiltonian the only non-zero Berry curvature components are $B^{n_g \varphi_0}(n_g, E_J)$ and $B^{\varphi_0 E_J}(n_g, E_J)$ which do not depend on the parameter φ_0 . Berry curvature components of the original Hamiltonian are then given by

$$\begin{aligned}B^{n_g \varphi_L} &= \frac{\partial E_J}{\partial \varphi_L} B^{n_g E_J} + \frac{\partial \varphi_0}{\partial \varphi_L} B^{n_g \varphi_0} \quad (\text{B.4}) \\ &= \frac{1 + \kappa \cos(\varphi_L - \varphi_R)}{1 + \kappa^2 + 2\kappa \cos(\varphi_L - \varphi_R)} B^{n_g \varphi_0}(n_g, E_J(\kappa, \varphi_L, \varphi_R)),\end{aligned}$$

$$\begin{aligned}B^{n_g \varphi_R} &= \frac{\partial E_J}{\partial \varphi_R} B^{n_g E_J} + \frac{\partial \varphi_0}{\partial \varphi_R} B^{n_g \varphi_0} \quad (\text{B.5}) \\ &= \frac{\kappa^2 + \kappa \cos(\varphi_L - \varphi_R)}{1 + \kappa^2 + 2\kappa \cos(\varphi_L - \varphi_R)} B^{n_g \varphi_0}(n_g, E_J(\kappa, \varphi_L, \varphi_R)),\end{aligned}$$

$$\begin{aligned}B^{\varphi_L \varphi_R} &= \frac{\partial E_J}{\partial \varphi_L} \frac{\partial \varphi_0}{\partial \varphi_R} B^{E_J \varphi_0} + \frac{\partial E_J}{\partial \varphi_R} \frac{\partial \varphi_0}{\partial \varphi_L} B^{\varphi_0 E_J} \quad (\text{B.6}) \\ &= \frac{\kappa E_J \sin(\varphi_L - \varphi_R)}{\sqrt{1 + \kappa^2 + 2\kappa \cos(\varphi_L - \varphi_R)}} B^{\varphi_0 E_J}(n_g, E_J(\kappa, \varphi_L, \varphi_R)).\end{aligned}$$

The eigenstates of a CPB can be expressed analytically using Mathieu functions $me_\nu(q, x)$ [11]

$$\psi_m(\varphi) = \frac{1}{\sqrt{2}} e^{in_g(\varphi - \varphi_0)} me_{-2[n_g - k(m, n_g)]} \left(-\frac{2E_J}{E_C}, \frac{\varphi - \varphi_0}{2} \right), \quad (\text{B.7})$$

where $k(m, n_g)$ is an integer function that is used to properly sort the eigenvalues and eigenstates as described in [11]. One can also use this formula to calculate the Berry curvature of a CPB and in turn the Berry curvature of a CPT. Corresponding eigenvalues are given by

$$E_m = \frac{E_C}{4} a_{2[n_g + k(m, n_g)]} \left(-\frac{2E_J}{E_C} \sqrt{1 + \kappa^2 + 2\kappa \cos(\varphi_L - \varphi_R)} \right), \quad (\text{B.8})$$

where $a_\nu(q)$ denotes Mathieu's characteristic value.

B.1 Berry Curvature in the Transmon Regime

When $E_J \gg E_C$ the ground state of a CPB Hamiltonian B.3 can be well approximated by the ground state of a harmonic oscillator which is given by

$$\psi_0(\varphi) = \left(\frac{E_J}{2\pi^2 E_C} \right)^{1/8} e^{in_g(\varphi - \varphi_0)} e^{-\sqrt{E_J/8E_C}(\varphi - \varphi_0)^2} \quad (\text{B.9})$$

$$\frac{\partial \psi_0}{\partial n_g} = i(\varphi - \varphi_0) \psi_0 \quad (\text{B.10})$$

$$\frac{\partial \psi_0}{\partial \varphi_0} = \left(-in_g + \sqrt{\frac{E_J}{2E_C}}(\varphi - \varphi_0) \right) \psi_0 \quad (\text{B.11})$$

$$\frac{\partial \psi_0}{\partial E_J} = \left(\frac{1}{8E_J} - \frac{1}{\sqrt{32E_J E_C}}(\varphi - \varphi_0)^2 \right) \psi_0 \quad (\text{B.12})$$

Using this we can calculate that in the lowest order the Berry curvature of a CPB in the transmon regime is given by $B^{n_g \varphi_0} = 1$, $B^{n_g E_J} = 0$ and $B^{E_J \varphi_0} = 0$. Then, using the formulas B.4, B.5, and B.6, we can calculate the Berry curvature of a CPT in the transmon regime to the lowest order

$$B^{n_g \varphi_L} = \frac{1 + \kappa \cos(\varphi_L - \varphi_R)}{1 + \kappa^2 + 2\kappa \cos(\varphi_L - \varphi_R)}, \quad (\text{B.13})$$

$$B^{n_g \varphi_R} = \frac{\kappa^2 + \kappa \cos(\varphi_L - \varphi_R)}{1 + \kappa^2 + 2\kappa \cos(\varphi_L - \varphi_R)}, \quad (\text{B.14})$$

$$B^{\varphi_L \varphi_R} = 0. \quad (\text{B.15})$$

We also note that these formulas are a good approximation over multiple bands since the corrections are exponentially suppressed in $\sqrt{E_J/E_C}$.

It is useful to expand the formula B.13 into a series in terms of κ , which is possible since we assume that $0 \leq \kappa < 1$. Formula B.13 is actually a generating function of the Chebyshev polynomials, so we can write

$$B^{n_g \varphi_L} = \sum_{n=0}^{\infty} T_n(-\cos(\varphi_L - \varphi_R)) \kappa^n = \sum_{n=0}^{\infty} (-1)^n \kappa^n \cos(n(\varphi_L - \varphi_R)), \quad (\text{B.16})$$

where T_n is the n -th Chebyshev polynomial of the first kind [10]. This is also the Fourier series of the Berry curvature.

C Response Quantization

We can expand the Berry curvature in the Fourier cosine series as

$$B^{n_g\varphi_L} = \sum_{n,m=0}^{+\infty} a_{nm} \cos(2n\pi n_g) \cos(m(\varphi_L - \varphi_R)). \quad (\text{C.1})$$

Depending on the form of the applied drives, we can calculate the contribution to the corresponding Fourier term that will determine the quantization of the circuit response.

Let us first consider the drives $n_g = r_g \cos(\omega_g t)$, $\varphi_L - \varphi_R = 2\pi r_\varphi \cos(\omega_0 t)$. We will make use of the following identity [1]

$$\cos(x \cos \theta) = J_0(x) + 2 \sum_{n=1}^{+\infty} (-1)^n J_{2n}(x) \cos(2n\theta), \quad (\text{C.2})$$

where J_n are Bessel functions, to write the Berry curvature as

$$\begin{aligned} B^{n_g\varphi_L} &= \sum_{n,m=0}^{+\infty} a_{nm} \cos(2n\pi r_g \cos(\omega_g t)) \cos(2m\pi r_\varphi \cos(\omega_0 t)) \quad (\text{C.3}) \\ &= \sum_{n,m=0}^{+\infty} a_{nm} \left[J_0(2\pi n r_g) + 2 \sum_{p=1}^{+\infty} (-1)^p J_{2p}(2\pi n r_g) \cos(2p\omega_g t) \right] \\ &\quad \times \left[J_0(2m\pi r_\varphi) + 2 \sum_{q=1}^{+\infty} (-1)^q J_{2q}(2m\pi r_\varphi) \cos(2q\omega_0 t) \right]. \end{aligned}$$

Berry current is then given by $I_g B^{n_g\varphi_L} = I_{g0} \sin(\omega_g t) B^{n_g\varphi_L}$ and we are interested in extracting the amplitude of the term $\sin(\omega_g t)$ from the Fourier expansion. If the ratio ω_g/ω_0 is irrational, this amplitude is given by

$$\begin{aligned} &\sum_{n,m=0}^{+\infty} a_{nm} (J_0(2n\pi r_g) + J_2(2n\pi r_g)) J_0(2m\pi r_\varphi) \quad (\text{C.4}) \\ &= 1 + \sum_{m=1}^{+\infty} a_{0m} J_0(2m\pi r_\varphi) + \sum_{n=1,m=0}^{+\infty} \frac{1}{n\pi r_g} a_{nm} J_1(2n\pi r_g) J_0(2m\pi r_\varphi), \end{aligned}$$

where we made use of the identity $J_{\alpha-1}(x) + J_{\alpha+1}(x) = 2\alpha J_\alpha(x)/x$ [1]. In a similar manner we can find that the amplitude in the case of the drive $n_g = r_g \cos(\omega_g t)$, $\varphi_L - \varphi_R = \omega_0 t$ is given by

$$\sum_{n=0}^{+\infty} a_{n0}(J_0(2n\pi r_g) + J_2(2n\pi r_g)) = 1 + \sum_{n=1}^{+\infty} \frac{1}{n\pi r_g} a_{n0} J_1(2n\pi r_g). \quad (\text{C.5})$$

For a large x , we can approximate the Bessel function as [1]

$$J_\alpha(x) \approx \sqrt{\frac{2}{\pi x}} \cos(x - \alpha\pi/2 - \pi/4). \quad (\text{C.6})$$

Applying this to our expressions for the response quantization [C.4](#), [C.5](#) we get that, for sufficiently large sweep amplitudes, the oscillations around perfect unit quantization drop off as $r_\varphi^{-1/2}$ and $r_g^{-3/2}$.

In the case of a rational ratio of frequencies $\omega_g/\omega_0 = p/q$, we numerically calculate the Fourier coefficient at ω_g over the period $T = pT_g = qT_0$.

Bibliography

- [1] Milton Abramowitz and Irene A. Stegun. *Handbook of Mathematical Functions with Formulas, Graphs, and Mathematical Tables*. ninth Dover printing, tenth GPO printing. New York: Dover, 1964.
- [2] J. Aumentado et al. “Nonequilibrium Quasiparticles and $2e$ Periodicity in Single-Cooper-Pair Transistors”. In: *Phys. Rev. Lett.* 92 (6 2004), p. 066802. DOI: [10.1103/PhysRevLett.92.066802](https://doi.org/10.1103/PhysRevLett.92.066802). URL: <https://link.aps.org/doi/10.1103/PhysRevLett.92.066802>.
- [3] P.-M. Billangeon et al. “ac Josephson Effect and Resonant Cooper Pair Tunneling Emission of a Single Cooper Pair Transistor”. In: *Phys. Rev. Lett.* 98 (21 2007), p. 216802. DOI: [10.1103/PhysRevLett.98.216802](https://doi.org/10.1103/PhysRevLett.98.216802). URL: <https://link.aps.org/doi/10.1103/PhysRevLett.98.216802>.
- [4] Lev S. Bishop. *Circuit Quantum Electrodynamics*. 2010. eprint: [arXiv:1007.3520](https://arxiv.org/abs/1007.3520).
- [5] Alexandre Blais et al. *Circuit Quantum Electrodynamics*. 2020. eprint: [arXiv:2005.12667](https://arxiv.org/abs/2005.12667).
- [6] Giuseppe Falci et al. “Detection of geometric phases in superconducting nanocircuits”. In: *Nature* 407.6802 (2000), pp. 355–358. ISSN: 1476-4687. DOI: [10.1038/35030052](https://doi.org/10.1038/35030052). URL: <https://doi.org/10.1038/35030052>.
- [7] Valla Fatemi, Anton R. Akhmerov, and Landry Bretheau. “Weyl Josephson circuits”. In: *Phys. Rev. Research* 3 (1 2021), p. 013288. DOI: [10.1103/PhysRevResearch.3.013288](https://doi.org/10.1103/PhysRevResearch.3.013288). URL: <https://link.aps.org/doi/10.1103/PhysRevResearch.3.013288>.
- [8] David J. Griffiths. *Introduction to Quantum Mechanics (2nd Edition)*. 2nd. Pearson Prentice Hall, Apr. 2004. ISBN: 0131118927. URL: <http://www.amazon.com/exec/obidos/redirect?tag=citeulike07-20&path=ASIN/0131118927>.
- [9] Tobias Herrig and Roman-Pascal Riwar. *A "minimal" topological quantum circuit*. 2020. eprint: [arXiv:2012.10655](https://arxiv.org/abs/2012.10655).
- [10] N. Karjanto. “Properties of Chebyshev polynomials”. In: (2020). eprint: [arXiv:2002.01342](https://arxiv.org/abs/2002.01342).
- [11] Jens Koch et al. “Charge insensitive qubit design derived from the Cooper pair box”. In: (2007). DOI: [10.1103/PhysRevA.76.042319](https://doi.org/10.1103/PhysRevA.76.042319). eprint: [arXiv:cond-mat/0703002](https://arxiv.org/abs/cond-mat/0703002).
- [12] Raphael Leone and Laurent Lévy. “Topological quantization by controlled paths: Application to Cooper pairs pumps”. In: *Phys. Rev. B* 77 (6 2008), p. 064524. DOI: [10.1103/PhysRevB.77.064524](https://doi.org/10.1103/PhysRevB.77.064524). URL: <https://link.aps.org/doi/10.1103/PhysRevB.77.064524>.

- [13] J. E. Mooij and Yu. V. Nazarov. “Superconducting nanowires as quantum phase-slip junctions”. In: *Nature Physics* 2.3 (2006), pp. 169–172. ISSN: 1745-2481. DOI: [10.1038/nphys234](https://doi.org/10.1038/nphys234). URL: <https://doi.org/10.1038/nphys234>.
- [14] Jukka P. Pekola et al. “Single-electron current sources: Toward a refined definition of the ampere”. In: *Rev. Mod. Phys.* 85 (4 2013), pp. 1421–1472. DOI: [10.1103/RevModPhys.85.1421](https://link.aps.org/doi/10.1103/RevModPhys.85.1421). URL: <https://link.aps.org/doi/10.1103/RevModPhys.85.1421>.
- [15] L. Peyruchat et al. “Transconductance quantization in a topological Josephson tunnel junction circuit”. In: *Phys. Rev. Research* 3 (1 2021), p. 013289. DOI: [10.1103/PhysRevResearch.3.013289](https://link.aps.org/doi/10.1103/PhysRevResearch.3.013289). URL: <https://link.aps.org/doi/10.1103/PhysRevResearch.3.013289>.
- [16] Roman-Pascal Riwar et al. “Multi-terminal Josephson junctions as topological matter”. In: *Nature Communications* 7.1 (2016), p. 11167. ISSN: 2041-1723. DOI: [10.1038/ncomms11167](https://doi.org/10.1038/ncomms11167). URL: <https://doi.org/10.1038/ncomms11167>.
- [17] Uri Vool and Michel Devoret. “Introduction to quantum electromagnetic circuits”. In: *International Journal of Circuit Theory and Applications* 45.7 (2017), pp. 897–934. DOI: <https://doi.org/10.1002/cta.2359>. eprint: <https://onlinelibrary.wiley.com/doi/pdf/10.1002/cta.2359>. URL: <https://onlinelibrary.wiley.com/doi/abs/10.1002/cta.2359>.
- [18] David J. van Woerkom, Attila Geresdi, and Leo P. Kouwenhoven. “One minute parity lifetime of a NbTiN Cooper-pair transistor”. In: *Nature Physics* 11.7 (2015), pp. 547–550. ISSN: 1745-2481. DOI: [10.1038/nphys3342](https://doi.org/10.1038/nphys3342). URL: <https://doi.org/10.1038/nphys3342>.
- [19] Di Xiao, Ming-Che Chang, and Qian Niu. “Berry phase effects on electronic properties”. In: *Rev. Mod. Phys.* 82 (3 2010), pp. 1959–2007. DOI: [10.1103/RevModPhys.82.1959](https://link.aps.org/doi/10.1103/RevModPhys.82.1959). URL: <https://link.aps.org/doi/10.1103/RevModPhys.82.1959>.